Velocity Profiles in Shear-Banding Wormlike Micelles

Jean-Baptiste Salmon, Annie Colin, and Sébastien Manneville
Centre de Recherche Paul Pascal, Avenue Schweitzer, 33600 Pessac, France

François Molino
Groupe de Dynamique des Phases Condensées, Université Montpellier II, Place E. Bataillon, 34095 Montpellier, France
(Received 19 November 2002; published 6 June 2003)

Using dynamic light scattering in heterodyne mode, we measure velocity profiles in a much studied system of wormlike micelles (CPCl/NaSal) known to exhibit both shear-banding and stress plateau behavior. Our data provide evidence for the simplest shear-banding scenario, according to which the effective viscosity drop in the system is due to the nucleation and growth of a highly sheared band in the gap, whose thickness linearly increases with the imposed shear rate. We discuss various details of the velocity profiles in all the regions of the flow curve and emphasize the complex, non-Newtonian nature of the flow in the highly sheared band.

DOI: 10.1103/PhysRevLett.90.228303 PACS numbers: 83.80.Qr, 47.50.+d, 83.60.–a, 83.85.Ei

Understanding the correlation between mechanical and structural response in non-Newtonian fluids submitted to high deformation rates is crucial on both fundamental and technological grounds [1]. Among the variety of complex fluids investigated in recent years, a wide class exhibits flow-structure coupling that leads to a strong shear-thinning behavior: along the steady-state flow curve (shear stress σ vs shear rate $\dot{\gamma}$), a drop of up to 3 orders of magnitude in the effective viscosity $\eta = \sigma/\dot{\gamma}$ is observed in a very narrow stress range leading to a stress plateau (for a review, see Refs. [1,2]).

A major breakthrough in the understanding of this stress plateau was reached when local scattering experiments revealed the existence of bands of different microstructures normal to the velocity gradient. These bands correspond to a new shear-induced structure (SIS). Such a structural *shear banding* has been observed in ordered mesophases (lamellar, hexagonal, cubic) [3], wormlike micelles [4,5], and transient gels [6].

However, global rheological data coupled to a local characterization of the microstructure are not sufficient to provide a complete picture of shear banding: a *local description* of the flow with high enough resolution is still missing, which makes detailed theoretical models somewhat speculative. In the simplest models of the velocity field along the stress plateau, the system is supposed to separate into two differently sheared bands: a weakly sheared region that flows at $\dot{\gamma}_1$ and a highly sheared region at $\dot{\gamma}_2$, $\dot{\gamma}_1$ ($\dot{\gamma}_2$) being the lower (upper) limit of the plateau. The high shear rate branch is assumed to grow and to progressively fill the gap at almost constant shear stress when the shear rate is increased [7,8]. Experimentally, this very basic issue of the nature of the flow field remains obscure. Indeed local velocity measurements by Callaghan and co-workers using nuclear magnetic resonance (NMR) [9] provide contradictory evidence with respect to this simple scenario: those measurements show the existence of narrow bands of high shear rate that do not necessarily appear at the point of highest shear stress within the cell.

In this Letter, we show that high-resolution local velocity measurements using dynamic light scattering (DLS) help to clarify the experimental situation on shear banding. We demonstrate that a picture with two bands and one sharp interface holds for the much studied wormlike micellar system CPCl/NaSal in brine. This corresponds to the simplest scenario, with the potentially important difference that the SIS under high shear rate exhibits strong non-Newtonian behavior. Since the pioneering work by Rehage and Hoffmann [10], this system has been demonstrated to exhibit both a stress plateau and optical birefringence shear banding [4]. Our main contribution relies on recording simultaneously the local velocity and global rheological data in Couette geometry along the whole flow curve. This enables us to demonstrate for the first time the nucleation of a highly sheared band at a critical stress and to follow its growth from the rotor to the stator as the shear rate spans the stress plateau. We show that the width of the band grows linearly with the shear rate, in agreement with the decrease of the measured effective viscosity, and that the SIS is not Newtonian.

Wormlike micellar systems consist of very long cylindrical aggregates of self-assembled surfactant molecules that mimic polymer solutions, but can dynamically break and recombine [10,11]. Generically, one starts from an isotropic viscoelastic solution of these micelles above the semidilute regime, which behaves like a Maxwell fluid at small deformations [1]. Upon increasing $\dot{\gamma}$ and entering the nonlinear regime, the onset of the stress plateau for a critical shear rate $\dot{\gamma}_1$ is associated with the nucleation and growth of highly birefringent bands, suggesting strong alignment of the micelles along the velocity direction [4,5]. As the shear rate is further increased above $\dot{\gamma}_1$, the

new organization progressively fills the gap at almost constant stress, up to a second critical shear rate $\dot{\gamma}_2$. Above $\dot{\gamma}_2$, the system enters a second regime of apparently homogeneous structure, with a second branch of increasing stress (see Fig. 1 for a typical flow curve).

Our system of wormlike micelles is a binary mixture of cetylpyridinium chloride (CP^+, Cl^-) and sodium salicylate (Na^+, Sal^-) in 0.5 M NaCl brine. We focus on a 6% wt. sample at 21.5 °C, in the domain above the semidilute regime (0.5–5% wt.) but far below the equilibrium isotropic-nematic (I-N) transition that occurs at $\phi_{IN} \approx$ 20% wt.

Rheological flow curves are measured using a stress imposed rheometer (TA Instruments AR 1000) and transparent Couette cells of outer radius $R_2 = 25$ mm and different gap widths e ($e = 1$ or 3 mm). To access local velocity, we use a heterodyne DLS technique that has been described elsewhere [12]. The measurement of the local velocity relies on performing the interference between a reference beam and light scattered from a small volume of the sample of typical size 50 μm. The correlation function of the interference signal exhibits oscillations at the Doppler frequency $\mathbf{q} \cdot \mathbf{v}$ where $\mathbf{q}$ is the scattering wave vector and $\mathbf{v}$ is the local velocity. Good statistical convergence is achieved by averaging the correlation function over 3 s. Velocity profiles $v(x)$ are measured by moving the rheometer along the velocity gradient (x axis) by steps of 30 μm, leading to a complete velocity profile in about 2 min. Typical uncertainties are about 5%.

In order to enhance the scattering properties of our system, we add a small amount (1% wt.) of 30 nm colloidal particles (Ludox from Aldrich). We checked that the rheological properties, particularly the plateau behavior, were not affected by the addition of those scatterers. Indeed, the small size of the scatterers compared to the mesh size of the micellar network ensures a negligible influence on the structural and mechanical behaviors of the sample.

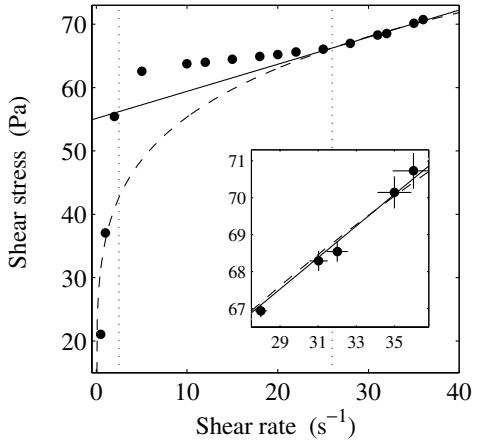

FIG. 1. Steady-state flow curve for a 6% wt. CPCl/NaSal solution in 0.5 M brine at 21.5 °C. The data were collected under controlled shear rate in a 1 mm gap Couette cell. Vertical lines indicate the limits of the banding domain. For $\dot{\gamma} > \dot{\gamma}_2 \approx 26\ s^{-1}$, the data were fitted by a power-law fluid $\sigma = 35.9\,\dot{\gamma}^{0.19}$ (dashed line) and by a Bingham fluid $\sigma = 55.1 + 0.43\dot{\gamma}$ (solid line). Inset: high shear branch; error bars account for the measured temporal fluctuations of σ and $\dot{\gamma}$.

Figure 1 shows the steady-state shear stress recorded in our micellar system using the shear-rate-imposed mode of the rheometer. This flow curve presents a stress plateau at $\sigma \approx 65$ Pa that extends from $\dot{\gamma}_1 \approx 2.5\ s^{-1}$ to $\dot{\gamma}_2 \approx 26\ s^{-1}$ corresponding to a drop in the effective viscosity by a factor of 10. Note that for $\dot{\gamma} \gtrsim \dot{\gamma}_2$, the stress response and the imposed shear rate are no longer strictly stationary: σ and $\dot{\gamma}$ fluctuate by about 2% around their mean values. These fluctuations may originate from the coupling between the feedback loop of the rheometer and flow instabilities occurring at high shear rates [4,7]. Indeed, at $\dot{\gamma} \approx 37\ s^{-1}$, the sample began to fracture so that no measurement is available at higher shear rates.

Figure 2 summarizes our main result. Velocity profiles in the gap are displayed for $\dot{\gamma}$ ranging from 1 to 28 s^{-1}. For all the shear rates in the plateau domain, the velocity profiles exhibit an unambiguous banding structure: two regions of different well-defined local shear rates coexist when $\dot{\gamma}_1 < \dot{\gamma} < \dot{\gamma}_2$. The highly sheared band nucleates on the inner wall of the Couette cell at the onset of the plateau and expands as $\dot{\gamma}$ is increased up to $\dot{\gamma}_2$ where the band fills the whole gap. As can be seen in Fig. 2, the local shear rate in the weakly sheared region remains constant and equal to $\dot{\gamma}_1 \approx 2.5\ s^{-1}$. Moreover, although significantly curved (see below), the velocity profiles in the highly sheared region are compatible with a constant local shear rate of $\dot{\gamma}_2 \approx 26\ s^{-1}$, leading to a viscosity ratio of about 10 that remains almost constant all along the plateau. Note that in all our data, no noticeable wall slip was observed.

These profiles also yield the width h of the highly sheared band. Figure 3(a) demonstrates that h increases linearly with $\dot{\gamma}$: $h = e\,(\dot{\gamma} - \dot{\gamma}_1)/(\dot{\gamma}_2 - \dot{\gamma}_1)$. This linear

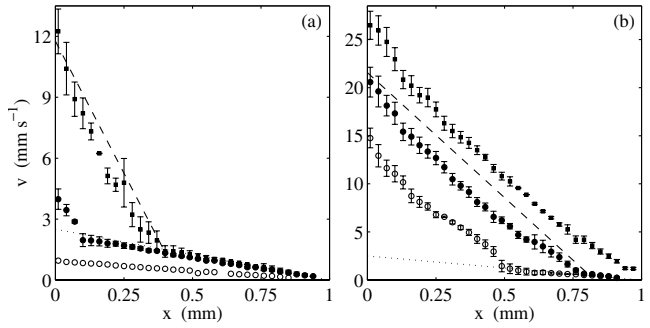

FIG. 2. Velocity profiles recorded while measuring the flow curve of Fig. 1. (a) $\dot{\gamma} = 1$ (○), 5 (●), and 12 s^{-1} (■). (b) $\dot{\gamma} = 15$ (○), 22 (●), and 28 s^{-1} (■). The value $x = 0$ ($x = 1$) corresponds to the rotor (stator). The dotted line is $v(x) = \dot{\gamma}_1\,(e - x)$ with $\dot{\gamma}_1 = 2.5\ s^{-1}$. The dashed lines correspond to a shear rate $\dot{\gamma}_2 = 26\ s^{-1}$.

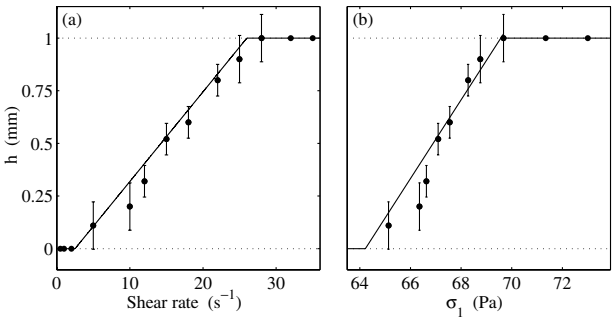

FIG. 3. Width h of the highly sheared band. (a) h vs $\dot{\gamma}$. With the value $\dot{\gamma}_1 = 2.5 \pm 0.2\ s^{-1}$ inferred from the velocity profiles of Fig. 2, a good linear approximation of $h(\dot{\gamma})$ is obtained with $\dot{\gamma}_2 = 26 \pm 1\ s^{-1}$ (solid line). (b) h vs σ_1. The solid line corresponds to Eq. (1) with $\sigma^\star = 64.2$ Pa.

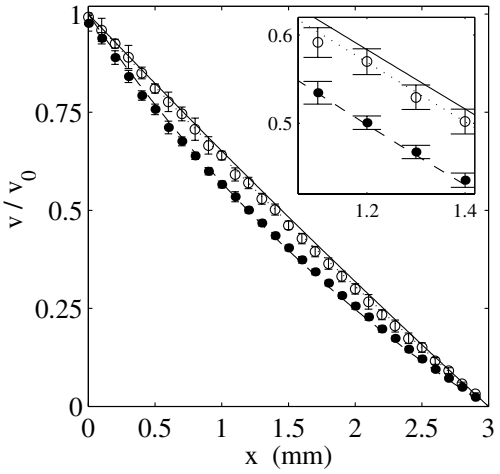

FIG. 4. Velocity profiles measured in the 3 mm gap Couette cell and rescaled by the rotor velocity v_0 for two values of $\dot{\gamma}$ below the banding transition. For $\dot{\gamma} = 1\ s^{-1}$ (○), the normalized data are well fitted using a weakly shear-thinning law $\sigma \sim \dot{\gamma}^{0.7\pm0.1}$ (dotted line) [15]. For $\dot{\gamma} = 2\ s^{-1}$ (●), a stronger shear-thinning behavior $\sigma \sim \dot{\gamma}^{0.28\pm0.03}$ provides a very good fit (dashed line). The average deviations from the fits are 2% and 3%, respectively. The solid line is the velocity profile expected for a Newtonian fluid. Inset: Blowup of the middle of the gap.

relation is just a consequence of the continuity of the velocity field between two regions of given shear rates $\dot{\gamma}_1$ and $\dot{\gamma}_2$ [7,8]. Figure 3(b) reveals a physically more relevant point: the increase of h vs σ is consistent with the assumption that the interface is stable at a given shear stress $\sigma^\star \approx 64$ Pa [13]. Indeed, in the Couette geometry where $\sigma(x) = \sigma_1[R_1/(R_1 + x)]^2$ (R_1 is the radius of the rotor and σ_1 the corresponding shear stress), this assumption leads to

$$h(\sigma_1) = R_1\left(\sqrt{\frac{\sigma_1}{\sigma^\star}} - 1\right) \approx \frac{R_1}{2}\frac{\sigma_1 - \sigma^\star}{\sigma^\star}, \qquad (1)$$

where the rightmost term results from the narrow-gap approximation ($e/R_1 \ll 1$). Note that taking into account the curvature of the Couette cell also implies that the stress slightly increases all along the coexistence domain consistently with Ref. [14] (see Fig. 1).

Beyond shear-banding evidence, our technique enables us to analyze in more detail the flow behavior of the material in the regions below and above the plateau. In Fig. 4 are displayed two normalized velocity profiles below the plateau at $\dot{\gamma} = 1\ s^{-1}$ and $\dot{\gamma} = 2\ s^{-1}$ in a 3 mm gap. For $\dot{\gamma} = 1\ s^{-1}$, the velocity profile is very close to a straight line, consistent with the Newtonian behavior of the micellar solution at low shear rates [4]. However, as shown in the inset of Fig. 4, our data do not exactly fall on the Newtonian velocity profile but rather present a small curvature which can be accounted for by the rheological behavior $\sigma \sim \dot{\gamma}^{0.7}$ [15]. When $\dot{\gamma} = 2\ s^{-1}$, i.e., just below the onset of shear banding at $\dot{\gamma}_1$, the curvature is much more pronounced and $\sigma \sim \dot{\gamma}^{0.28}$ leads to a perfect fit of the velocity profile. This demonstrates the existence of weak shear thinning on the low shear branch, that sharply increases as the banding transition is approached.

Looking more closely at the velocity profiles in the plateau region, one notes that the highly sheared band displays a significant curvature even in a 1 mm gap [see Fig. 2(b)]. The same observation holds for velocity profiles recorded at $\dot{\gamma} > \dot{\gamma}_2$ where the SIS has completely invaded the gap. This shows that the SIS cannot be described by a Newtonian fluid. More precisely, this curvature can be linked to the global rheological behavior of the SIS. Indeed, the flow curve of Fig. 1 for $\dot{\gamma} > \dot{\gamma}_2$ is very well fitted by either a power law $\sigma = A\dot{\gamma}^n$ or a Bingham fluid $\sigma = \sigma_0 + A\dot{\gamma}$ [see inset of Fig. 1] [1]. The very same rheological behaviors account rather well for the curvature of all the velocity profiles at $\dot{\gamma} > \dot{\gamma}_2$ with the parameters (n, A) or (σ_0, A) inferred from the global rheology (see Fig. 5 for $\dot{\gamma} = 28$ and $32\ s^{-1}$). Note that the Bingham behavior is suggested from the analogy with other related viscoelastic systems, whose similar nonlinear behavior has been interpreted in terms of a steady system of bulk fractures [6]. Here, the range of $\dot{\gamma}$ on the high shear branch is limited to 26–37 s^{-1} so that we cannot discriminate between the two above behaviors. Since temporal fluctuations of the velocity field also come into play, only further studies will help to select the correct non-Newtonian relation for the high shear branch.

Let us now discuss the present results in light of previous studies concerning wormlike micellar systems. To our knowledge, our measurements provide the first clear evidence for shear banding in micellar solutions. However, recent local NMR velocity measurements by Fischer and Callaghan [16] lead to a radically different description of the flow field. Reference [16] suggests the nucleation and growth of a gel whereas our data clearly shows the coexistence of two different well-defined shear bands flowing at $\dot{\gamma}_1$ and $\dot{\gamma}_2$, respectively. These important discrepancies may be explained by the fact that the distances to the I-N transition are drastically different in the

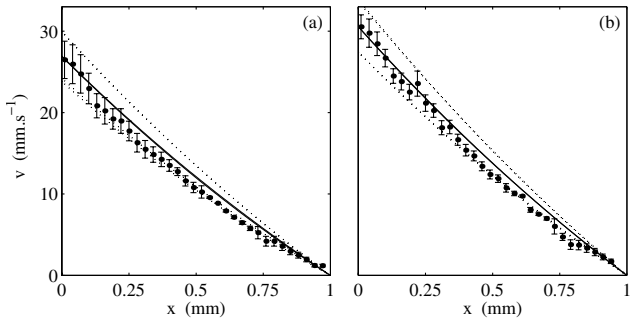

FIG. 5. Velocity profiles in the high shear branch at (a) $\dot{\gamma} = 28\ \mathrm{s}^{-1}$, $\sigma = 66.9$ Pa, and (b) $\dot{\gamma} = 32\ \mathrm{s}^{-1}$, $\sigma = 68.5$ Pa. In each case, two solid lines correspond to two different but indistinguishable velocity profiles corresponding to (i) a power-law behavior $\sigma = 35.9\dot{\gamma}^{0.19}$ and (ii) a Bingham behavior $\sigma = 55.1 + 0.43\dot{\gamma}$ [15]. The average deviations from the fits are 11% and 9%, respectively. The dotted lines account for the measured global stress fluctuation of 2%.

systems under study: CTAB/D_2O at 20% wt. for which $\phi_{\mathrm{IN}} \approx 21\%$ wt. in Ref. [16], and CPCl/NaSal in brine at 6% wt. for which $\phi_{\mathrm{IN}} \approx 20\%$ wt. in our case. Moreover, rapid temporal fluctuations occur in the high shear rate branch which might make the analysis of the NMR measurements very difficult since one hour is required to obtain a velocity profile using NMR. Definite conclusions on that issue are left to future work.

More generally, our results can be analyzed in the broader framework of complex fluid flows. Indeed, it appears that many complex fluids with sometimes radically different microstructures display shear-banding behaviors similar to those discussed in the present Letter [17,18]. Such behaviors are usually observed in the vicinity of a shear-induced transition: pasty-fluidized state transition in soft glassy materials [17] or shear-thickening transition for highly dilute micellar systems [18]. It is henceforth quite clear that phenomenological approaches should be looked for as in Refs. [8,13,14]. However, in all the above experimental systems, the nature and the rheological behavior of the SIS are still under debate. We believe that non-Newtonian features, such as those revealed in this Letter for the highly sheared structure, may prove most relevant in the understanding of those inhomogeneous flows.

Another robust experimental fact is the presence of temporal fluctuations and flow instabilities in a lot of systems that display structural shear banding and/or inhomogeneous velocity profiles. For instance, in our system, flow instabilities lead to fractures at high shear rates and to the expulsion of the sample from the rheometer [4,7]. Such dynamical behaviors have been reported in other systems: foams, granular pastes, and surfactant systems [17–19]. Thus, purely spatial approaches appear as insufficient. This suggests to look for a spatiotemporal picture of complex fluid flows near shear-induced transitions with intermittent, localized, or even chaotic events. We believe that further experimental work should focus on this particular point and that theoretical models should involve both temporal and spatial degrees of freedom.

The authors thank J.-F. Berret, C. Gay, and P. Olmsted for fruitful discussions.

[1] R. G. Larson, *The Structure and Rheology of Complex Fluids* (Oxford University, Oxford, 1999).
[2] *Soft and Fragile Matter: Nonequilibrium Dynamics, Metastability and Flow*, edited by M. E. Cates and M. R. Evans (IOP, Bristol, U.K., 2000).
[3] D. Roux *et al.*, Europhys. Lett. **24**, 53 (1993); L. Ramos *et al.*, Langmuir **16**, 5846 (2000); E. Eiser *et al.*, Phys. Rev. E **61**, 6759 (2000).
[4] J.-F. Berret *et al.*, J. Phys. II **4**, 1261 (1994); Phys. Rev. E **55**, 1668 (1997); S. Lerouge *et al.*, Phys. Rev. Lett. **81**, 5457 (1998).
[5] V. Schmitt *et al.*, Langmuir **10**, 955 (1994).
[6] F. Molino *et al.*, J. Phys. Condens. Matter **12**, A491 (2000).
[7] N. A. Spenley *et al.*, Phys. Rev. Lett. **71**, 939 (1993); M. E. Cates *et al.*, Europhys. Lett. **21**, 451 (1993).
[8] P. D. Olmsted and C.-Y. D. Lu, Phys. Rev. E **56**, 55 (1997).
[9] R.W. Mair and P.T. Callaghan, Europhys. Lett.. **36**, 719 (1996); M. M. Britton and P.T. Callaghan, Phys. Rev. Lett. **78**, 4930 (1997); Eur. Phys. J. B **7**, 237 (1999).
[10] H. Rehage and H. Hoffmann, Mol. Phys. **74**, 933 (1991).
[11] M. E. Cates, Macromolecules **20**, 2289 (1987).
[12] J.-B. Salmon *et al.*, Eur. Phys. J. Appl. Phys. **22**, 143 (2003).
[13] C.-Y. D. Lu *et al.*, Phys. Rev. Lett. **84**, 642 (2000).
[14] O. Radulescu and P. D. Olmsted, J. Non-Newtonian Fluid Mech. **91**, 143 (2000).
[15] The velocity profile for the rheological law $\sigma \sim \dot{\gamma}^n$ in Couette geometry is $v(x) = r\frac{n}{2}[\frac{\sigma_1}{A}(\frac{R_1}{R_2})^2]^{1/n}[(\frac{R_2}{r})^{2/n} - 1]$, where $r = R_1 + x$ is the radial position, R_1 (R_2) is the radius of the rotor (stator). For the case of a Bingham fluid $\sigma = \sigma_0 + A\dot{\gamma}$, the velocity profile reads $v(x) = r\frac{\sigma_1}{2A}(\frac{R_1}{R_2})^2[(\frac{R_2}{r})^2 - 1] + r\frac{\sigma_0}{A}\ln(\frac{r}{R_2})$.
[16] E. Fischer and P.T. Callaghan, Phys. Rev. E **64**, 011501 (2001).
[17] G. Debrégeas *et al.*, Phys. Rev. Lett. **87**, 178305 (2001); P. Coussot *et al.*, Phys. Rev. Lett. **88**, 218301 (2002); F. Pignon *et al.*, J. Rheol. **40**, 573 (1996).
[18] C.-H. Liu and D. J. Pine, Phys. Rev. Lett. **77**, 2121 (1996); P. Boltenhagen *et al.*, Phys. Rev. Lett. **79**, 2359 (1997).
[19] E. K. Wheeler *et al.*, J. Non-Newtonian Fluid Mech. **75**, 193 (1998); R. Bandyopadhyay *et al.*, Phys. Rev. Lett. **84**, 2022 (2000); A.-S. Wunenburger *et al.*, Phys. Rev. Lett. **86**, 1374 (2001).